The Journal of Immunology

Constitutive Lck Activity Drives Sensitivity Differences between CD8 $^{+}$ Memory T Cell Subsets

Duane Moogk, Shi Zhong, Zhiya Yu, Ivan Liadi, William Rittase, Victoria Fang, Janna Dougherty, Arianne Perez-Garcia, Iman Osman, Cheng Zhu, Navin Varadarajan, Nicholas P. Restifo, Alan B. Frey and Michelle Krogsgaard

J Immunol 2016; 197:644-654; Prepublished online 6 June 2016;
doi: 10.4049/jimmunol.1600178
http://www.jimmunol.org/content/197/2/644

This information is current as of October 21, 2020.

Supplementary Material **http://www.jimmunol.org/content/suppl/2016/06/04/jimmunol.1600178.DCSupplemental**

References This article **cites 71 articles**, 29 of which you can access for free at:
http://www.jimmunol.org/content/197/2/644.full#ref-list-1

Why *The JI*? Submit online.

- **Rapid Reviews! 30 days*** from submission to initial decision
- **No Triage!** Every submission reviewed by practicing scientists
- **Fast Publication!** 4 weeks from acceptance to publication

**average*

Subscription Information about subscribing to *The Journal of Immunology* is online at:
http://jimmunol.org/subscription

Permissions Submit copyright permission requests at:
http://www.aai.org/About/Publications/JI/copyright.html

Email Alerts Receive free email-alerts when new articles cite this article. Sign up at:
http://jimmunol.org/alerts

The Journal of Immunology is published twice each month by
The American Association of Immunologists, Inc.,
1451 Rockville Pike, Suite 650, Rockville, MD 20852
Copyright © 2016 by The American Association of Immunologists, Inc. All rights reserved.
Print ISSN: 0022-1767 Online ISSN: 1550-6606.

Downloaded from http://www.jimmunol.org/ by guest on October 21, 2020

Constitutive Lck Activity Drives Sensitivity Differences between CD8$^+$ Memory T Cell Subsets

Duane Moogk,* Shi Zhong,*,[1] Zhiya Yu,[†] Ivan Liadi,[‡] William Rittase,[§] Victoria Fang,*,[¶] Janna Dougherty,* Arianne Perez-Garcia,*,[2] Iman Osman,*,[‖] Cheng Zhu,[§] Navin Varadarajan,[‡] Nicholas P. Restifo,[†] Alan B. Frey,[#] and Michelle Krogsgaard*,**

CD8$^+$ T cells develop increased sensitivity following Ag experience, and differences in sensitivity exist between T cell memory subsets. How differential TCR signaling between memory subsets contributes to sensitivity differences is unclear. We show in mouse effector memory T cells (T_{EM}) that >50% of lymphocyte-specific protein tyrosine kinase (Lck) exists in a constitutively active conformation, compared with <20% in central memory T cells (T_{CM}). Immediately proximal to Lck signaling, we observed enhanced Zap-70 phosphorylation in T_{EM} following TCR ligation compared with T_{CM}. Furthermore, we observed superior cytotoxic effector function in T_{EM} compared with T_{CM}, and we provide evidence that this results from a lower probability of T_{CM} reaching threshold signaling owing to the decreased magnitude of TCR-proximal signaling. We provide evidence that the differences in Lck constitutive activity between CD8$^+$ T_{CM} and T_{EM} are due to differential regulation by SH2 domain–containing phosphatase-1 (Shp-1) and C-terminal Src kinase, and we use modeling of early TCR signaling to reveal the significance of these differences. We show that inhibition of Shp-1 results in increased constitutive Lck activity in T_{CM} to levels similar to T_{EM}, as well as increased cytotoxic effector function in T_{CM}. Collectively, this work demonstrates a role for constitutive Lck activity in controlling Ag sensitivity, and it suggests that differential activities of TCR-proximal signaling components may contribute to establishing the divergent effector properties of T_{CM} and T_{EM}. This work also identifies Shp-1 as a potential target to improve the cytotoxic effector functions of T_{CM} for adoptive cell therapy applications. ***The Journal of Immunology*****, 2016, 197: 644–654.**

T cell effector functions are initiated by ligation of the TCR with an MHC-presenting Ag peptide (pMHC) on the surface of an APC (1). T cell sensitivity is substantially increased following Ag experience, and maturation and can vary between Ag-experienced memory subsets (2), which has been attributed in part to enhanced TCR-proximal signaling (3). Central memory (T_{CM}) and effector memory (T_{EM}) T cells have unique gene expression and cytokine signaling signatures (4), which result in distinct effector capacities (5). As a result, T_{CM} have an enhanced ability to confer host protection against viral and bacterial challenge (6) as well as enhanced therapeutic antitumor responses compared with T_{EM} (7). However, T_{EM} possess greater in vitro cytotoxic properties (8), which suggests that the superior in vivo properties of T_{CM} result from greater proliferation upon Ag re-encounter and preferential homing to secondary lymphoid tissues (7, 9) despite a deficiency in cytotoxic properties compared with T_{EM} (9). The contributions of TCR signaling components that confer differences in activation sensitivity and functional outcomes between CD8$^+$ T_{CM} and T_{EM} remain unclear.

Initiation of T cell signaling by TCR ligation leads to a sequence of well-characterized signaling events, including lymphocyte-specific protein tyrosine kinase (Lck) phosphorylation of CD3 ITAMs (10) and Zap-70 (11). Active Lck is present in T cells prior to TCR stimulation (12) and exists in equilibrium between four states, based on phosphorylation of activating Y394 and inhibitory Y505 (12). It is unclear whether the level of constitutively active Lck differs significantly between T cell subsets, and whether any such differences in Lck activity would contribute to establishing

*Laura and Isaac Perlmutter Cancer Center, New York University School of Medicine, New York, NY 10016; [†]Center for Cancer Research, National Cancer Institute, National Institutes of Health, Bethesda, MD 20892; [‡]Department of Chemical and Biomolecular Engineering, University of Houston, TX 77004; [§]George W. Woodruff School of Mechanical Engineering, Georgia Institute of Technology, Atlanta, GA 30332; [¶]New York University Medical Scientist Training Program, New York, NY 10016; [‖]Ronald Perelman Department of Dermatology, New York University School of Medicine, New York, NY 10016; [#]Department of Cell Biology, New York University School of Medicine, New York, NY 10016; and **Department of Pathology, New York University School of Medicine, New York, NY 10016

[1]Current address: Life Sciences Center, Xiangxue Pharmaceutical Co., Ltd., Guangzhou, China.

[2]Current address: Kite Pharma, Santa Monica, CA.

ORCIDs: 0000-0003-3742-5902 (Z.Y.); 0000-0003-3830-6569 (I.L.); 0000-0003-4268-3148 (W.R.); 0000-0001-9376-1279 (V.F.); 0000-0002-1718-565X (C.Z.); 0000-0001-7524-8228 (N.V.).

Received for publication January 29, 2016. Accepted for publication May 4, 2016.

This work was supported by National Institutes of Health Grant 1U01CA137070 (to M.K.), R24 OD018339-01 (to M.K.), R01 CA174385 (to N.V.), and R01 CA108573 (to A.B.F.), American Cancer Society Research Scholar Grant RSG-09-070-01-LIB (to M.K.) and Grant CPRIT RP130570 (to N.V.), a Cancer Research investigator grant (to M.K.), a Pew Scholar in Biomedical Sciences grant from the Pew Trust (to M.K.), National Institute of General Medical Sciences Grant 5R01GM085586-04 (to M.K.), an Intramural Research Program grant from the National Institutes of Health, National Cancer Institute, and Center for Cancer Research (to N.P.R.), New York University Cancer Institute Cancer Center Support Grant 5P30CA016087-27 (to I.O.), and by a grant from the Marc Jacobs campaign to support the Interdisciplinary Melanoma Cooperative Group (to I.O.).

Address correspondence and reprint requests to Dr. Michelle Krogsgaard, New York University School of Medicine, 522 First Avenue, Smilow 1311, New York, NY 10016. E-mail address: Michelle.Krogsgaard@nyumc.org

The online version of this article contains supplemental material.

Abbreviations used in this article: Cbp, Csk-binding protein; Csk, C-terminal Src kinase; DIC, differential interference contrast; IP, immunoprecipitate; Lck, lymphocyte-specific protein tyrosine kinase; pMHC, peptide–MHC complex; Shp-1, SH2 domain–containing phosphatase-1; T2-A2Kb, T2 APC expressing chimeric A*0201/H2K^b; T_{CM}, central memory T cell; T_{EM}, effector memory T cell.

Copyright © 2016 by The American Association of Immunologists, Inc. 0022-1767/16/$30.00

Downloaded from http://www.jimmunol.org/ by guest on October 21, 2020

differential Ag sensitivities. This premise is supported by recent work by Manz et al. (13), which showed that increasing Lck activity through inhibition of C-terminal Src kinase (Csk) leads to enhanced downstream signaling following T cell stimulation. In the present study, we show that T_{CM} and T_{EM} possess differential constitutive Lck activities, driven in part by differential regulation by SH2 domain–containing phosphatase-1 (Shp-1) and Csk. In response to the moderate affinity (9.3 μM) self-antigen $gp100_{209–217(2M)}$, differences in proximal T cell signaling resulted in significantly different probabilities of T_{CM} and T_{EM} achieving full cytotoxic effector function. Comparatively higher constitutive Lck activity can explain the more robust proximal Ag-dependent signaling and cytotoxic effector function of T_{EM}. Given the importance of both TCR dwell time and Lck in driving TCR signaling (14), our results suggest that T cell sensitivity may be influenced by constitutive Lck activity, which varies sufficiently between T_{CM} and T_{EM} to establish differential Ag sensitivities.

Materials and Methods

Reagents and materials

All cells were cultured in RPMI 1640 L-glutamine–supplemented media (Life Technologies) with the inclusion of 10% FBS (Thermo Scientific), sodium pyruvate, MEM nonessential amino acids, and penicillin/streptomycin (Life Technologies). Anti-Lck (SPM413 and 2102), anti–pY394-Lck (Tyr^{394}), anti–pTyr^{505}-Lck (pY505.4), anti-GST (K-18), anti–Zap-70 (1E7.2), anti–Shp-1 (C19), anti-Csk (C-20), anti–Csk-binding protein (Cbp; PAG-C1), anti–rabbit IgG F(ab′)$_2$-allophycocyanin, anti–mouse IgG F(ab′)$_2$-FITC, and normal rabbit IgG isotype control were from Santa Cruz Biotechnology. FITC-conjugated anti-CD8a (53-6.7), PerCp-Cy5.5–conjugated anti-CD44 (IM7), and PE-conjugated CD62L (MEL-14) were from eBioscience. Anti–pShp-1 (S591) and anti–pShp-1 (Y536) were from ECM Biosciences. Anti–pZap-70 (Y319) and anti–pShp-1 (Y564) were from Cell Signaling Technology. Anti-pY142 (K25-407.69) and anti-Themis (Q1-1103) were from BD Pharmingen. Anti-rabbit IRDye 680LT, anti-goat IRDye 680LT, and anti-mouse 800CW IRDye were from LI-COR Biosciences. Allophycocyanin–anti-mouse IgG (poly4053) was from BioLegend. Anti-phosphotyrosine (4G10) was from Millipore. Anti-actin was from Acris Antibodies. Anti-Cbp (EPR9705) was from Abcam. rCD3-ζ with N-terminal GST tag was from Novus Biologicals. ProLong Gold antifade with DAPI, fura 2-AM, LysoTracker Red, and calcein green AM was from Life Technologies. $gp100_{209–217(2M)}$ peptide (IMDQVPFSV) was from Bio-Synthesis.

Animals and cell culture

JR209 T_{CM} and T_{EM} were obtained as previously described (15). Major lymph nodes and spleens were extracted from the humanized transgenic JR209 mouse (16) and mechanically digested, followed by lysis of the RBC population with ACK lysis buffer (Life Technologies). Isolated lymphocytes were cultured at an initial concentration of 5×10^6 cells/ml with 1 μM $gp100_{209–217(2M)}$ and 20 ng/ml IL-15 or IL-2 (R&D Systems) (17, 18) and passaged 1:2 every other day with replenishment of media and 10 ng/ml cytokine. At day 6 of culture, live cells were purified by density gradient centrifugation with Ficoll-Paque Plus (GE Healthcare), washed and resuspended at 2×10^6 cells/ml, and allowed to rest for at least 3 h or overnight before use in serum-free media. The phenotypes of T_{CM} ($CD44^{hi}$, $CD62L^{hi}$) and T_{EM} ($CD44^{hi}$, $CD62L^{lo}$) were verified by flow cytometry (Fig. 1A). For analysis of memory subsets obtained from aged JR209 mice, lymphocytes were obtained from lymph nodes and spleen of 10- to 12-mo-old mice, as described above, followed by $CD8^+$ lymphocyte enrichment (Stemcell Technologies).

T2 APCs expressing chimeric A*0201/$H2K^b$ (T2-A2Kb), a gift from Dr. L. Sherman (Scripps Research Institute), were maintained in culture at 0.5×10^6 cells/ml in the presence of G418 selective agent (Life Technologies) and loaded with peptide overnight at the indicated concentrations. Mice were housed in specific pathogen-free conditions at the Smilow Research Center Animal Facility (New York University) and Taconic Biosciences (Hudson, NY). All animal experiments were performed in accordance with protocols approved by the New York University Institutional Animal Care and Use Committee.

Chromium release cytotoxicity assay

Bulk T cell cytotoxicity was assessed by chromium release assay, as previously described (19). Peptide-loaded (at indicated concentrations), ^{51}Cr-labeled T2-A2Kb APCs and T cells were cultured in round-bottom 96-well plates at the ratios indicated for 6 h at 37°C. Positive control (maximum release) wells included 5% Triton X-100 solution in the absence of T cells, whereas negative control (spontaneous release) wells contained APCs only. Supernatant (100 μl) from each well was transferred to a 96-well isoplate (PerkinElmer) and 100 μl OptiPhase SuperMix scintillation fluid (PerkinElmer) was added and thoroughly mixed and gamma radiation detected with a MicroBeta^2 microplate counter (PerkinElmer). Specific lysis was calculated as (counts per minute of experimental release − counts per minute of spontaneous release)/(counts per minute of maximum release − counts per minute of spontaneous release). For quantification of cytotoxicity following Shp-1 inhibition, cells were treated with 50 μM NSC-87877 (Calbiochem) overnight and washed three times prior to addition of APCs.

Quantification of effector molecule expression by RT-PCR

Total RNA was extracted from resting T cells using an RNeasy kit (Qiagen). cDNA was synthesized using a first-strand cDNA synthesis kit (Roche) using oligo-p$(dT)_{15}$ primer. Quantitative PCR and analysis were performed using the LightCycler 480 (Roche) with Probes Master and TaqMan probes (Life Technologies) specific for granzyme B, perforin, and Fas ligand and hypoxanthine phosphoribosyltransferase as housekeeping gene. Relative expression was quantified as fold change in expression relative to naive T cells.

Granule polarization imaging

T cells were labeled with 50 nM LysoTracker Red in complete media for 30 min at 37°C. T cells and peptide-loaded APCs were combined in phenol red–free RPMI 1640 plus 10% FBS in a single well of an eight-chambered borosilicate coverglass system (Nunc), treated with 10% poly-L-lysine for 10 min (Sigma-Aldrich). Differential interference contrast (DIC) and fluorescence images were collected at 20-s intervals for 6 h with an Axiovert 200 inverted microscope (Zeiss) and ×40 oil objective (EC Plan-Neofluar, 1.3 numerical aperture, Zeiss) housed at 37°C/5% CO_2. Images were acquired with a CoolSNAP HQ^2 camera (Photometrics). For analysis, T cell/APC conjugates were orientated using DIC images and a grid was created to identify the quadrant of the T cell that included the T cell/APC interface. The polarization time was determined as the time when 80% of the LysoTracker signal is in the front quadrant. Image acquisition and analysis were performed using MetaMorph microscopy automation and image analysis software (Molecular Devices).

Time-lapse imaging microscopy in nanowell grids

For the time-lapse imaging microscopy in nanowell grids assay for detection of serial killing events, T cell/APC interactions and cytotoxic kinetics were performed on microfabricated nanowells, as previously described (20, 21). Nanowell arrays were fabricated on a glass-bottom petri dish (Ted Pella, 14027-200). T cells and peptide-loaded T2-A2Kb APCs were labeled with PKH67 and PKH26 dyes (Sigma-Aldrich), respectively. Furthermore, T_{EM} was additionally labeled with Vybrant violet dye (Life Technologies) to differentiate between T_{CM} and T_{EM}. Subsequently, T_{CM}, T_{EM}, and APCs were loaded onto nanowell arrays and imaged for 6 h at 5-min intervals under 37°C/5% CO_2 with a ×20 air objective (Plan-Apochromat ×20/0.8 Ph2 M27) and ORCA flash 4.0 camera (Hamamatsu). Annexin V–Alexa Fluor 647 (Life Technologies) was added to dynamically track APC apoptosis. Raw images were analyzed using scripts for automated image preprocessing and segmentations (22). Resulting data were then analyzed using Excel, Access, and GraphPad Prism to identify and record serial killing events of interest.

Imaging of T cell cytotoxic efficiency

For imaging of T cell cytotoxic efficiency, T cell and peptide-loaded APCs were cultured as described for "Granule polarization imaging," except 2×10^5 JR209 T cells and 1×10^5 peptide-loaded T2-A2Kb APCs were imaged for 8 h, acquired at 3-min intervals with a ×40 air objective (LD Plan-Neofluar, 0.6 numerical aperture, Zeiss). For analysis, initial T cell/APC conjugation and APC death were manually identified, and T cell/APC conjugates lasting >10 min were analyzed. Cytotoxic efficiency was calculated as (T cell/APC conjugates that result in APC lysis)/(total stable T cell/APC conjugates observed). Image acquisition and analysis were performed using MetaMorph microscopy automation and image analysis software (Molecular Devices).

Calcium flux imaging

Imaging of T cell calcium flux was performed as previously described (23, 24). T cell and peptide-loaded APCs were cultured and imaged as described for "Granule polarization imaging," except T cells were treated

Downloaded from http://www.jimmunol.org/ by guest on October 21, 2020

with fura 2-AM dye before combining with peptide-loaded T2-A2Kb APCs. Images were acquired under DIC illumination, as well as detection at 510 nm from both 340 and 380 nm excitation with a ×40 oil objective (EC Plan-Neofluar, 1.3 numerical aperture, Zeiss). Image acquisition and analysis were performed using MetaMorph microscopy automation and image analysis software (Molecular Devices). The ratio of the fura 2-AM emission intensity at 510 nm resulting from 340 and 380 nm excitation was determined to quantify the relative intracellular calcium concentration. Relative calcium concentration is reported as the integrated whole-cell average 340/380 ratio of intensities for 5 min following T cell/APC conjugation.

Western blot analysis

T cells were lysed in ice-cold lysis buffer containing 20 mM Tris-HCl (pH 7.5), 150 mM NaCl, 1% *n*-dodecyl-β-D-maltoside, 1 mM Na_3VO_4, plus complete protease inhibitor mixture (Roche) and phosphatase inhibitor mixture 2 (Sigma-Aldrich) for 30 min at 4˚C, and clarified by centrifugation at 16,000 × *g* for 15 min at 4˚C and collection of supernatant. Lysate was separated by SDS-PAGE, transferred to nitrocellulose membranes, and quantified by near-infrared fluorescence with the Odyssey imaging system (LI-COR Biosciences). For quantification of protein phosphorylation, values were calculated as the intensity of phosphorylated-specific Ab over intensity of total protein-specific Ab, normalized to unity for T_{CM}. For quantification of all other proteins, values were calculated as the intensity of the protein of interest over intensity of actin loading control, normalized to unity for T_{CM}. For phospho–Zap-70 time course experiments, values were calculated as the intensity of phospho–Zap-70 over the intensity of total Zap-70, normalized to time 0 and relative to maximum value attained by either cell type.

For assessment of phosphorylation of Zap-70 after activation, T cells and peptide-loaded T2-A2Kb APCs were combined at a ratio of 2:1, centrifuged briefly to induce conjugation, and incubated at 37˚C. At indicated times, ice-cold PBS was added and cells were pelleted and immediately lysed and then assessed by Western blot as described above. For assessment of Cbp phosphorylation, lysates were incubated with anti-Cbp Ab overnight at 4˚C, followed by incubation with protein A/G beads for 4 h at 4˚C. Beads were washed twice with lysis buffer and once with water prior to addition of an equal volume of Laemmli buffer, and assessed by Western blot analysis as described above. For assessment of Themis association with Shp-1, immunoprecipitation with Shp-1–specific Ab was performed exactly as described for Cbp. Blots were probed with both Shp-1– and Themis-specific Abs and quantified as the intensity of Themis over the intensity of Shp-1, normalized to unity for T_{CM}.

Calculation of the percentage of Lck phosphorylated at Y394 was performed as previously described (12). Following clarification, lysates were precleared by incubation with protein A/G beads (Pierce) for 2 h at 4˚C, then incubation with either anti–pY394-Lck Ab or isotype control IgG overnight at 4˚C, followed by depletion of protein–Ab complexes by incubation with protein A/G beads for 4 h at 4˚C. Depleted lysate was separated by SDS-PAGE, transferred to nitrocellulose membranes, and quantified by near-infrared fluorescence with the Odyssey imaging system (LI-COR Biosciences). The percentage of Lck that is phosphorylated at Y394 was calculated as: (Lck depleted/pY394 depleted) × 100, where Lck depleted = 1 − (intensity of Lck from pY394 immunoprecipitate [IP]/intensity of Lck from control IP, and pY394 depleted = 1 – (intensity of pY394 from pY394 IP/intensity of pY394 from control IP).

Kinase activity of immunoprecipitated Lck was determined as previously described (12). Cells were lysed and precleared as above, immunoprecipitated with either anti-Lck Ab or isotype control IgG and incubated with protein A/G beads as above. Beads were washed twice in lysis buffer, then washed twice and suspended in 20 μl kinase buffer containing 20 mM Tris-HCl (pH 7.5), 10 mM $MgCl_2$, 10 mM $MnCl_2$, 1 mM ATP, and 100 ng recombinant GST-tagged rCD3-ζ and incubated for 60 min at 37˚C. Laemmli buffer was added directly to samples, boiled for 5 min, separated by SDS-PAGE, transferred to nitrocellulose membranes, and quantified by near-infrared fluorescence with the Odyssey imaging system. Lck kinase activity was calculated as (pY142 intensity from Lck IP/GST intensity from Lck IP)/(pY142 intensity from control IP/GST intensity from control IP).

Quantification of Shp-1 phosphatase activity

Cells were lysed in buffer containing 50 mM Tris (pH 8), 10 mM EDTA, 150 mM NaCl, and 1% Nonidet P-40 plus protease and phosphatase inhibitors. Clarified lysates were incubated overnight with protein A magnetic beads (Bio-Rad) preincubated with 5 μg Shp-1 Ab, as per the manufacturer's instructions. The immune complexes were washed twice with lysis buffer without phosphatase inhibitors and twice with phosphatase assay buffer (62 mM HEPES (pH 5), 6.25 mM EDTA, 12.5 mM DTT). Immune complexes were then incubated in 200 μl phosphatase assay buffer plus 25 mM p-nitrophenyl phosphate for 30 min at 30˚C under shaking. After centrifugation to removed immune complexes, 800 μl 1 N NaOH was added to the supernatants and the OD was measured at 410 nm. The corresponding immune complexes, bound to protein A–Sepharose, were then analyzed by SDS-PAGE and immunodetection of Shp-1 was performed by Western blotting. Phosphatase activity was calculated by normalizing the OD 410 nm values to the amount of Shp-1 immunoprecipitated, as quantified by Western blot.

Colocalization analysis

For in vitro–derived JR209 T_{CM} and T_{EM}, cells were individually (T_{CM} or T_{EM}) cultured on 10% poly-L-lysine–treated coverslips for 30 min at room temperature, fixed with 4% paraformaldehyde for 15 min at room temperature, washed twice with 2% BSA in PBS, and permeabilized with 0.1% Triton X-100 for 7 min at room temperature. Cells were then washed twice and blocked with 5% BSA in PBS for 2 h at room temperature and incubated with primary Abs for Lck and Shp-1 for 1 h at room temperature or overnight at 4˚C, washed twice and then incubated with secondary Abs (anti–rabbit IgG $F(ab')_2$-allophycocyanin, anti–mouse IgG $F(ab')_2$-FITC) for 15 min at 4˚C and washed twice. Antifade with DAPI was added and coverslips were mounted on microscope slides. Images were collected at room temperature on a Leica TCS SP_5II confocal microscope with ×63 oil objective (Leica HC PL APO, numerical aperture 1.40) and Leica HyD detector using Leica LAS AF software. Colocalization analysis was performed on background-subtracted confocal images using ImageJ software (National Institutes of Health), and the Pearson correlation coefficient (R_r) was obtained using the JACoP plugin.

For in vivo–derived JR209 T_{CM} and T_{EM}, $CD8^+$-enriched cells were cultured on coverslips as above. Prior to fixation, cells were incubated with PerCp-Cy5.5–conjugated anti-CD44 and PE-conjugated anti-CD62L for 20 min at room temperature. Cells were then washed, fixed, permeabilized, and stained for Lck and Shp-1 as described above. For analysis, cells were first identified as either T_{CM} ($CD44^+$, $CD62L^{hi}$) or T_{EM} ($CD44^+$, $CD62L^{lo}$). The threshold whole cell–integrated PE intensity to distinguish between CD62L high versus low was determined by calculating the percentage of T_{CM} and T_{EM} in similarly stained cells by flow cytometry, and then determining the PE intensity that separated the analyzed cells into similarly proportioned populations. Colocalization analysis was then similarly performed as described above.

Flow cytometry

For evaluation of Lck, pY394 Lck, pY505 Lck, Shp-1, and pS591 Shp-1 expression in in vivo–derived JR209 T_{CM} and T_{EM}, lymphocytes were collected from the lymph nodes and spleens of 8- to 10-mo-old mice and $CD8^+$ T cells were purified by negative separation, as described above. T cells were stained with FITC-conjugated anti-CD8, PerCP-Cy5.5–conjugated anti-CD44, and PE-conjugated anti-CD62L Abs prior to being fixed with Fix Buffer I (BD Biosciences) and permeabilized with Perm Buffer III (BD Biosciences) as instructed by the supplier. Cells were then stained with Ag-specific Abs in PBS with 2% FBS, followed by allophycocyanin-conjugated species-appropriate IgG. Samples were collected on an LSR II flow cytometer (BD Biosciences) and analyzed using FlowJo X 10.0.7 flow cytometry analysis software (Tree Star). T_{CM} were identified as $CD44^{hi}$, $CD62L^{hi}$ and T_{EM} as $CD44^{hi}$, $CD62L^{lo}$.

Markov chain modeling (Lck come&stay model)

The equations governing the Markov chain model were extrapolated from the "Lck come&stay/signal duration" model developed by Chakraborty and colleagues (14). The model assumes an absorbing state once a CD8 molecule bound to an active Lck (Y394) binds to the TCR–pMHC complex. Relevant parameters were taken from literature (14, 25, 26) or experimentally derived in this study. The equations were numerically solved using MATLAB (MathWorks).

Statistical analysis

Statistical analysis was performed using a Student *t* test. A Mann–Whitney *U* test was performed for single-cell measurements where indicated. Individual cytotoxic efficiency experiments were assessed by a difference in proportions test for independent samples. In all cases, p values <0.05 were considered statistically significant. Error bars represent SEM unless otherwise stated. For box plots, the bottom and top of box represent the first and third quartiles, respectively; internal line represents the second quartile (median); and lower and upper whiskers represent the minimum and maximum data values, respectively.

Downloaded from http://www.jimmunol.org/ by guest on October 21, 2020

Results

Inferior CD8$^+$ T_{CM} cytotoxicity is due to an absence of cytotoxic granule delivery in a greater fraction of T cell/APC conjugates compared with T_{EM}

To address the role of activation signaling affecting the sensitivity of CD8$^+$ memory T cell effector function, we determined the cytotoxic properties of T_{CM} and T_{EM} in a well-characterized model system, that is, the humanized TCR-transgenic mouse model JR209, consisting of mouse T cells expressing the human R6C12 α/β TCR variable regions spliced onto mouse constant regions (16), recognizing the anchor-modified melanoma differentiation tissue-associated Ag $gp100_{209–217(2M)}$ (27) presented by chimeric A*0201/H2K^b (28). T_{CM} and T_{EM} were derived through in vitro Ag experience and exposure to IL-15 and IL-2, respectively (15, 29) (Fig. 1A). This method has been used previously to polarize CD8$^+$ T cells reactive toward foreign viral Ag (29) and tumor/self Ag (7, 15, 30), and for preparation of cells in the clinical setting (31, 32), and it is thus an established model for in vitro production of Ag-specific memory subsets resulting in populations representative of expected T_{CM} and T_{EM} phenotypes. We measured cytotoxicity by chromium release assay (Fig. 1B), which showed that T_{EM} had significantly higher specific lysis than did T_{CM}, consistent with established trends of CD8$^+$ T_{CM} and T_{EM} (7, 8, 33).

Expression of cytotoxic effector molecules correlates with cytotoxic activity of CD8$^+$ T cells (34). We therefore considered that higher T_{EM}-specific lysis could be due to higher expression and delivery of cytotoxic effector molecules. RT-PCR analysis of granzyme B, perforin, and Fas ligand (Fig. 1C) revealed that T_{EM} had greater expression of granzyme B compared with T_{CM}, although not for Fas ligand and perforin. It was unclear whether the lower levels of granzyme B in T_{CM} would be solely responsible for their lower specific lysis. Therefore, we quantified the delivery of cytotoxic granules by JR209 T_{CM} and T_{EM} by live cell fluorescence microscopy of T cells stained with granule-labeling LysoTracker Red interacting with T2-A2Kb presenting $gp100_{209–217(2M)}$ (Supplemental Fig. 1A). The time for effector molecules to polarize to the T cell/APC interface following conjugation was similar for T_{CM} and T_{EM} (Supplemental Fig. 1B). Notably, in both T_{CM} and T_{EM} >95% of T cell/APC conjugates that achieved polarization of effector molecules resulted in APC lysis. Combined, this suggests that lower T_{CM}-specific lysis may not be due to suboptimal expression or delivery of effector molecules, but rather an absence of effector molecule polarization altogether in a larger fraction of T_{CM}. This may result from insufficient activation signaling in T_{CM}, as granule recruitment and polarization along the centrosome depend on the strength of TCR signal (35).

To explore this idea further, we observed T cell/APC interactions by single-cell imaging to quantify the kinetics of T_{CM} and T_{EM} cytotoxicity. Greater cytotoxicity of T_{EM} could be caused by the ability of individual T_{EM} to kill multiple target cells, possibly due to greater expression of effector molecules (36). Profiling of the interactions between individual T cells and multiple APCs utilizing time-lapse imaging microscopy in nanowell grids (20, 21) revealed that T_{EM} were more likely to serially kill APCs (Fig. 1D). Although this could explain T_{EM} greater overall specific lysis, when we considered T cell interactions with single APCs, T_{EM} had a significantly higher cytotoxic efficiency (the fraction of stable T cell/APC conjugates that result in APC lysis) than did T_{CM} (Fig. 1E), suggesting that T_{CM} are less efficient at inducing APC lysis. Collectively, these results suggest that lower T_{CM} cytotoxic properties are due to a lesser ability to serially kill APCs, but also a lower efficiency at inducing APC apoptosis upon T cell/APC conjugation. Therefore, differences in cytotoxicity between

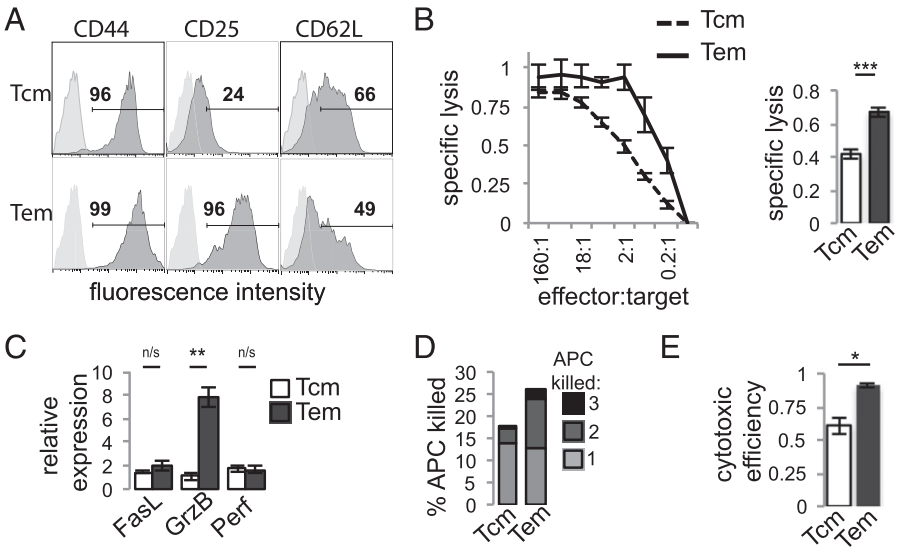

FIGURE 1. Superior JR209 T_{EM} cytotoxic function compared with T_{CM} is due to increased serial killing by T_{EM} and a greater likelihood of induction of effector molecule polarization. (**A**) Analysis of T_{CM} and T_{EM} phenotypic markers CD44, CD25, and CD62L by flow cytometry. (**B**) Cytotoxic properties of JR209 T_{CM} (dashed line) and T_{EM} (solid line) toward T2-A2Kb APCs loaded with 10 μM $gp100_{209–217(2M)}$ at E:T ratios indicated (*left*). Plot is representative of triplicate experiments. Specific lysis of T_{CM} and T_{EM} toward T2-A2Kb APCs loaded with 10 μM $gp100_{209–217(2M)}$ at a 2:1 E:T ratio is shown (*right*). Specific lysis was calculated as described in *Materials and Methods* (n = 6, two-tailed t test, $p < 0.0001$). (**C**) Expression of Fas ligand (FasL), granzyme B (GrzB), and perforin (Perf) by JR209 T_{CM} (open bars) and T_{EM} (filled bars) was determined by RT-PCR and presented as expression relative to naive JR209 T cells (n = 3, two-tailed t test, FasL p = 0.38, GrzB p = 0.002, Perf p = 0.84). (**D**) Serial killing by JR209 T_{CM} and T_{EM} of T2-A2Kb APCs loaded with 10 μM $gp100_{209–217(2M)}$ at 1:3 T cell/APC ratio. Values represent the number of APCs killed as a percentage of total APCs, grouped by the number of APCs killed by each individual T cell. (**E**) Cytotoxic efficiency (the fraction of stable T cell/APC conjugates that resulted in APC lysis) of JR209 T_{CM} and T_{EM} when cultured with T2-A2Kb APCs loaded with 10 μM gp100 at 1:1 T cell/APC ratio (n = 3; two-tailed t test, p = 0.01, difference in proportions test for each experiment, $p < 0.03$ for each). *$p < 0.05$, **$p < 0.005$, ***$p < 0.001$.

Downloaded from http://www.jimmunol.org/ by guest on October 21, 2020

T_{CM} and T_{EM} might be due to differential strengths of activation signaling, as increased avidity of interaction between the T cell and target APC correlates to increased levels of target cell death (37, 38). Overall, these data suggest that $CD8^+$ T_{CM} and T_{EM} have distinct properties affecting the strength of activation signaling and the probability of inducing cytotoxic effector function.

$CD8^+$ T_{EM} have higher levels of activation-induced Zap-70 phosphorylation and calcium signaling compared with T_{CM}

The magnitude of TCR-proximal signaling induced by TCR ligation correlates with T cell activation and functional performance (12, 39). We considered that the decreased fraction of T_{CM} that achieve cytotoxic effector function compared with T_{EM} might be due to lower TCR-proximal signaling. We quantified activation-induced phosphorylation of Zap-70 following JR209 T_{CM} and T_{EM} incubation with T2-A2Kb presenting $gp100_{209–217(2M)}$ by Western blot analysis (Fig. 2A). T_{EM} achieved higher Zap-70 phosphorylation than did T_{CM} during 5 min of T cell/APC conjugation (Fig. 2B).

We next quantified activation-induced cytoplasmic calcium influx by single-cell imaging of fura 2-AM–labeled T_{CM} and T_{EM} (Fig. 2C), as the quality of upstream TCR signaling quantitatively affects calcium influx (40). T_{EM} attained higher calcium levels than did T_{CM} (Fig. 2D). Notably, for both memory subsets, every stable T cell/APC conjugation resulted in elevation of T cell cytoplasmic calcium at least 70% above baseline levels, with the vast majority of cells reaching >100% above baseline levels (Fig. 2E), although T_{EM} achieved significantly higher maximum levels. Therefore, all observed T_{CM}/APC and T_{EM}/APC conjugates achieved some degree of TCR-dependent signaling, whereas only 61% of T_{CM} induce APC lysis, compared with 91% of T_{EM} (Fig. 1C). This suggests that the degree of activation signaling is insufficient to induce complete cytotoxic effector function in a larger fraction of T_{CM}.

Previous studies have shown that the threshold for APC killing is higher than that for calcium influx (41), such that calcium signaling can still be induced from a stimulus that is too weak to induce APC killing. Therefore, the magnitude of TCR signaling, not its absence, appears to be the source of lower cytotoxic effector function in T_{CM}. Furthermore, based on Zap-70 phosphorylation, the differences in T_{CM} and T_{EM} appear to arise very early in activation signaling.

$CD8^+$ T_{EM} have higher levels of constitutive Lck activity compared with T_{CM}

The role of Lck as the primary initiator of CD3 ITAM and Zap-70 phosphorylation following TCR ligation is well established (10, 42). Given the differences between T_{CM} and T_{EM} in phosphorylation of Zap-70, we investigated the role of Lck in driving functional differences between T_{CM} and T_{EM}. It has been suggested that the active pool of Lck in resting T cells could be promptly used to initiate signaling following TCR ligation (12). We hypothesized that differential levels of constitutive Lck activity between T_{CM} and T_{EM} could lead to differential signaling following TCR ligation. We compared the phosphorylation of both Lck Y394 and Lck Y505 in resting JR209 T_{CM} and T_{EM} by Western blot analysis, which showed that relative to T_{CM}, T_{EM} had greater levels of pY394 and lower levels of pY505 (Fig. 3A), suggesting that resting T_{EM} may have higher levels of active Lck. We also assessed Lck phosphorylation in T_{CM} and T_{EM} derived in vivo from aged (10–12 mo) JR209 mice (43). Flow cytometry analysis revealed that T_{EM} have higher levels of pY394 and lower levels of pY505 relative to T_{EM} (Fig. 3B). Therefore, in both in vitro–generated and in vivo–derived resting $CD8^+$ memory T cells, T_{EM} have higher phosphorylation of activating Lck Y394 and lower phosphorylation of inhibitory Lck Y505 compared with T_{CM}, suggesting that a higher amount of Lck is constitutively active in T_{EM}.

Previous calculations of Lck phosphorylation showed that ~38% of Lck was phosphorylated at Y394 in unsorted naive human $CD4^+$ T cells, and ~50% was phosphorylated in immortalized Jurkat cell line (12). To determine how $CD8^+$ T_{CM} and T_{EM}

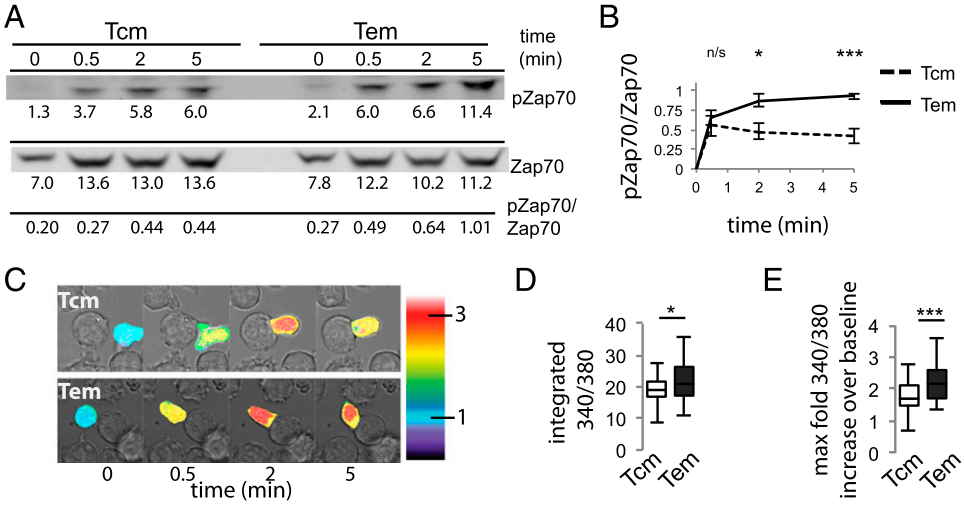

FIGURE 2. Greater activation signaling in JR209 T_{EM} compared with T_{CM}. (**A**) Western blot analysis of phosphorylated Zap-70 of JR209 T_{CM} and T_{EM} following activation by T2-A2Kb APCs loaded with 10 μM $gp100_{209–217(2M)}$. Values under blots are background-subtracted integrated intensity of bands × 1/100. (**B**) Quantification of Western blots for T_{CM} (dashed line) and T_{EM} (solid line) (n = 6, two-tailed t test, 0.5 min, p = 0.555, 2 min, p = 0.012, 5 min, p = 0.0004). (**C**) Live cell imaging of fura 2-AM–labeled JR209 T_{CM} and T_{EM} measuring relative calcium concentration following conjugation with T2-A2Kb APCs loaded with 10 μM $gp100_{209–217(2M)}$ (representative images shown). Calcium concentration relative to time 0, measured as the average whole-cell intensity of 340/380 emission intensities, is illustrated by a false color scale indicated by the color bars. (**D**) Integrated relative calcium concentrations for JR209 T_{CM} and T_{EM} during 5 min following T cell/APC conjugation (means, T_{CM} = 19.0, T_{EM} = 22.0; data are representative of triplicate experiments; T_{CM} n = 49, T_{EM} n = 47. Mann–Whitney U test, p = 0.023). (**E**) Maximum relative calcium concentration above time 0 baseline concentration attained during 5 min following T cell/APC conjugation, represented as fold increase from baseline value (means, T_{CM} = 1.80, T_{EM} = 2.21; data are representative of triplicate experiments; T_{CM} n = 49, T_{EM} n = 47. Mann–Whitney U test, $p < 0.0001$). *$p < 0.05$, ***$p < 0.001$.

Downloaded from http://www.jimmunol.org/ by guest on October 21, 2020

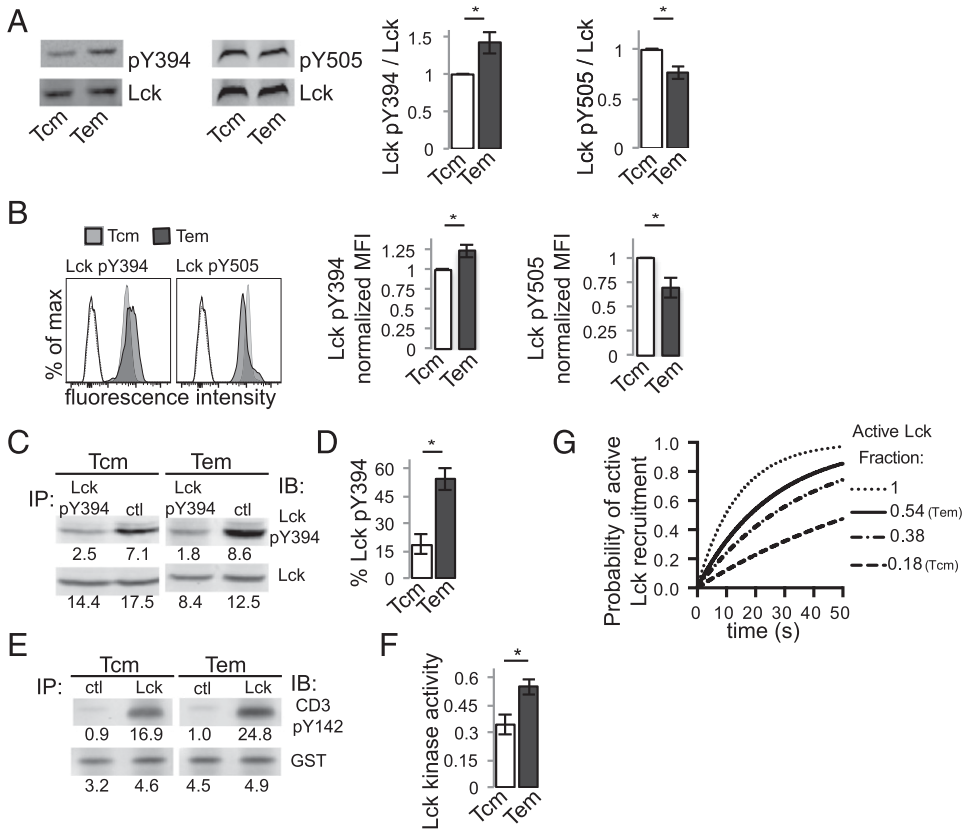

FIGURE 3. JR209 T_{CM} and T_{EM} have different constitutive Lck phosphorylation and Lck kinase activity. (**A**) Western blot analysis of total cell lysate of JR209 T_{CM} and T_{EM} for phosphorylated Lck Y394 and phosphorylated Lck Y505 (representative images shown on *left*). Quantified data (*right*) represent intensity of phosphorylated-specific Ab over intensity of total Lck-specific Ab, normalized to unity for T_{CM} (for pY394, $n = 13$, two-tailed t test, $p = 0.007$, for pY505, $n = 4$, two-tailed t test, $p = 0.036$). (**B**) Flow cytometry of Lck expression in in vivo–generated JR209 T_{CM} (gray) and T_{EM} (black) (representative plots shown on *left*). Unfilled profiles represent unstained controls for T_{CM} (dashed line) and T_{EM} (solid line) with the inclusion of allophycocyanin-labeled secondary Ab. Quantified data (*right*) represents mean fluorescence intensity normalized to unity for T_{CM} (for pY394, $n = 3$, two-tailed t test, $p = 0.043$, for pY505, $n = 3$, two-tailed t test, $p = 0.044$). (**C**) Lck Y394 phosphorylation as determined by immunoprecipitation with Lck pY394 or control IgG Ab, followed by Western blot analysis of depleted lysate for pY394 Lck and total Lck. (**D**) Quantification of Lck Y394 phosphorylation from (C) ($n = 4$, two-tailed t test, $p = 0.005$). (**E**) Lck kinase activity as determined by immunoprecipitation with Lck or control IgG Ab, followed by incubation with GST-tagged rCD3-ζ and ATP and Western blot analysis of pCD3-ζ (Y142) and GST. (**F**) Quantification of rCD3-ζ phosphorylation from (E), normalized to GST ($n = 3$, two-tailed t test, $p = 0.024$). (**G**) Simulation of the probability of forming an active TCR complex as a function of pMHC–TCR lifetime given the differences in Lck activity between T_{CM} (0.18) and T_{EM} (0.54), based on the Lck come&stay/signal duration model (14). For comparison, complete Lck activity (1.0) and the Lck activity previously calculated (12) for human naive CD4 T cells (0.38) are also included. *$p < 0.05$.

compare with these cell types, we calculated the amount of pY394 as a percentage of total Lck by immunoprecipitation and Western blot analysis of the resulting depleted lysate (Fig. 3C) (12). In T_{EM}, 54% of Lck is pY394, compared with T_{CM}, in which 18% of Lck is pY394 (Fig. 3D). Although our calculations for JR209 T_{EM} are similar to values previously calculated for naive human $CD4^+$ T cells and Jurkat cells (12), the calculated values for T_{CM} are significantly lower, suggesting that there is heterogeneity in constitutive Lck phosphorylation between these $CD8^+$ memory T cell subsets.

We next determined Lck kinase activity by quantifying the phosphorylation of recombinant CD3 ζ-chain by Lck immunoprecipitated from resting JR209 T_{CM} and T_{EM} lysates (12) (Fig. 3E). Correlative to Lck phosphorylation, T_{EM} have higher Lck kinase activity compared with T_{CM} (Fig. 3F). These data combine to suggest that T_{CM} and T_{EM} possess distinct levels of constitutive Lck phosphorylation and activity. As such, T_{EM} may be more poised to initiate signaling following TCR ligation, quantitatively affecting the degree of ITAM and Zap-70 phosphorylation and subsequent signal amplification, and thus the probability of inducing effector molecule polarization and cytotoxic effector function.

To consider the significance of the differences in Lck activity between T_{CM} and T_{EM}, we used a recently published model of T cell activation, the Lck come&stay/signal duration model (14), which posits that coreceptor-mediated delivery of active Lck to the pMHC–TCR complex is the most proximal limiting step in a kinetic proofreading model of T cell activation (44). The probability of forming an active TCR complex is considerably higher for T_{EM} compared with T_{CM}, and it more closely resembles the probability profiles for both Jurkat cells and naive human $CD4^+$ T cells (12) (Fig. 3G, Supplemental Fig. 2). This model suggests that, in a stochastic model of T cell activation (26, 45–47), small changes in the amount of active Lck may significantly affect the probability of formation of a signal-activating pMHC–TCR complex.

Differential regulation of constitutive Lck activity in $CD8^+$ T_{CM} and T_{EM}

To understand the mechanistic basis driving the differences in T_{CM} and T_{EM} Lck activity, we determined the extent of Lck interaction with Shp-1 and Csk, which affect Lck activity by dephosphorylation of Lck Y394 (48) and phosphorylation of Lck Y505 (49), respectively. The cellular localization of Shp-1 and Csk are me-

Downloaded from http://www.jimmunol.org/ by guest on October 21, 2020

diated by their interaction with Themis and Cbp, respectively (50). Western blot analysis revealed no significant differences in the expression of Shp-1, Csk, Themis, or Cbp in JR209 T_{CM} and T_{EM}, although Themis showed a trend toward higher expression in T_{EM} (Supplemental Fig. 3A). However, differences in cellular localization of Shp-1 or Csk could result in differential association with, and regulation of, Lck. We determined the colocalization of Lck with Shp-1 and Csk in JR209 T_{CM} and T_{EM} by confocal imaging and calculation of the Pearson coefficient. Both Shp-1 and Csk had higher colocalization with Lck in T_{CM} compared with T_{EM} (Fig. 4A, 4B), suggesting increased interactions of these negative regulatory molecules with Lck in T_{CM}. Colocalization analysis was also performed with in vivo–derived JR209 T_{CM} and T_{EM}, which showed similar results for both Shp-1 and Csk (Fig. 4C), further suggesting that Shp-1 and Csk may have a greater influence on Lck phosphorylation in T_{CM} compared with T_{EM}.

To determine how the interaction of both Csk and Shp-1 with Lck differs between T_{CM} and T_{EM}, we looked at their known interaction partners Cbp and Themis, respectively. Cbp is a membrane protein that brings Csk to the membrane and in closer proximity to Lck in a phosphorylation-dependent manner (50). Immunoprecipitation of Cbp followed by Western blot analysis using a phospho-tyrosine–specific Ab revealed that Cbp was similarly phosphorylated in T_{CM} and T_{EM} (Supplemental Fig. 3B). Shp-1 constitutively interacts with Themis in a GRB2-dependent manner (51). To examine the interaction of Shp-1 with Themis, we immunoprecipitated Shp-1 from T_{CM} and T_{EM} lysate and quantified both Shp-1 and Themis by Western blot analysis (Supplemental Fig. 3C). T_{EM} showed a slightly higher amount of Themis pulled down with Shp-1, although this was not a statistically significant difference from T_{CM}. Therefore, it does not appear that the amount of Shp-1 in complex with Themis, nor the amount of Csk associated to Cbp, accounts for differences in their localization and interaction with Lck between T_{CM} and T_{EM}.

Constitutive Shp-1 S591 phosphorylation causes both decreased phosphatase activity and decreased membrane localization (52), whereas phosphorylation of Y536 and Y564 result in increased phosphatase activity (53). Western blot analysis revealed that JR209 T_{EM} have higher Shp-1 pS591 compared with T_{CM} (Fig. 4D), a trend that was also observed in in vivo–derived JR209 T_{CM} and T_{EM} (Fig. 4E). No differences were observed for Y536 or Y534 (Supplemental Fig. 3D), which supports our observation that Shp-1 complexes with Themis/Grb2 similarly in T_{CM} and T_{EM}, as phosphorylation of both of these sites promotes interaction with Grb2 (54). We next determined Shp-1 phosphatase activity by quantifying the hydrolysis of *p*-nitrophenyl phosphate to *p*-nitrophenol by Shp-1 immunoprecipitated from resting JR209 T_{CM} and T_{EM} lysates. Correlative to Shp-1 phosphorylation, T_{EM} have lower Shp-1 phosphatase activity compared with T_{CM} (Fig. 4F). Together with our colocalization data (Fig. 4A–C), this suggests that in T_{EM} Shp-1 has decreased phosphatase activity and membrane localization compared with T_{CM}, and this may contribute to differences in Shp-1 interaction with, and dephosphorylation of, Lck Y394 in resting T cells.

To further address this possibility, we quantified Lck Y394 phosphorylation in resting JR209 T_{CM} and T_{EM} following incubation with the Shp-1 inhibitor NSC-87877. Western blot analysis revealed that NSC-87877 treatment eliminated the differences in Lck pY394 between T_{CM} and T_{EM} (Fig. 4G). Furthermore, analysis of cytotoxicity of T_{CM} and T_{EM} following incubation with NSC-87877 resulted in a significant increase in specific lysis by T_{CM} with minimal increase in T_{EM}-specific lysis over a range of E:T ratios (Fig. 4H). Specifically, at an E:T ratio of 2.5:1, inhibition of Shp-1 resulted in an average increase in specific lysis of 36% for T_{CM} compared with only 7% for T_{EM}. Collectively, these data provide further evidence that Shp-1 contributes to the differences in constitutive Lck activity and effector function between T_{CM} and T_{EM} (55) by disproportionately affecting T_{CM}.

Taken together, these results suggest that constitutive Lck activity, regulated by Shp-1 and Csk, differs between JR209 T_{CM} and T_{EM}, contributing to differences in TCR activation signaling and the probability of formation of a signal-activating pMHC–TCR complex.

Discussion

The role of constitutive Lck activity in the relative responsiveness of memory T cell subsets has not been studied. We show that differences in constitutive Lck activity between T_{CM} and T_{EM} result from differential interactions with and activity of Shp-1, and we also suggest a role for Csk. Modeling of TCR-proximal activation signaling suggests that these differences lead to T_{EM} being better poised to initiate TCR-proximal signaling immediately following TCR ligation.

The functional roles T_{CM} and T_{EM} in recall responses are still being clarified, although it is clear that these subsets differ in a number of properties, including expression of surface makers, tissue localization, recall proliferation, cytokine production, and cytotoxic activity (7, 56–59). Our results suggest that T_{EM} cytotoxic superiority may be due to differences in activation signaling and not just expression of effector molecules. However, it is well established that T_{CM} are functionally better than T_{EM} in terms of proliferation and cytokine production, specifically IL-2 (7, 8, 33). Consolidating this with our conclusion that T_{CM} achieve lower levels of TCR signaling and cytotoxic effector function is important to understand the divergent properties and functions of $CD8^+$ T cell memory subsets. The downstream pathways that drive cytokine production and proliferation are distinct (39), and although proliferative responses show a dependence on the degree of CD3 ITAM phosphorylation, similar cytokine responses are initiated with varying degrees of ITAM phosphorylation (39). Determining how the signaling pathway of cytotoxic effector function activation diverges from proliferative and cytokine production pathways will help to understand how T_{CM} and T_{EM} attain their characteristic functional properties.

In this study, we show that Lck activity influences the frequency of T_{CM} versus T_{EM} achieving threshold signaling to induce granule polarization and cytotoxic effector function. Importantly, in nearly all cases where polarization of effector molecules was observed, in both T_{CM} and T_{EM}, APC lysis was observed. Thus, cytotoxic effector function is an all-or-none proposition, such that lower overall levels of cytotoxic function by T_{CM} are due to a greater fraction of T_{CM}/APC conjugates not achieving sufficient signaling to induce effector molecule polarization, compared with T_{EM}. However, higher expression of effector molecules may enable T_{EM} to more effectively serially kill target cells, further contributing to their superior cytotoxic function. Analogous all-or-none results have been reported for recall proliferation of memory T cells, wherein an invariant threshold for the induction of proliferation exists, and the frequency of T cells reaching the signaling threshold was dependent on Ag dose (60). In our study, the distinguishing factor that affects the frequency of T_{CM} versus T_{EM} reaching the signaling threshold to induce cytotoxic effector function when exposed to similar Ag dose is instead Lck activity. Other factors, including Ag dose and TCR affinity, would affect the probability of achieving sufficient signaling to induce effector function (61). Therefore, the extent that constitutive Lck activity affects memory T cell sensitivity may depend on these factors, such that Lck activity may have a diminishing effect on T cell sensitivity with increasing TCR affinity.

Downloaded from http://www.jimmunol.org/ by guest on October 21, 2020

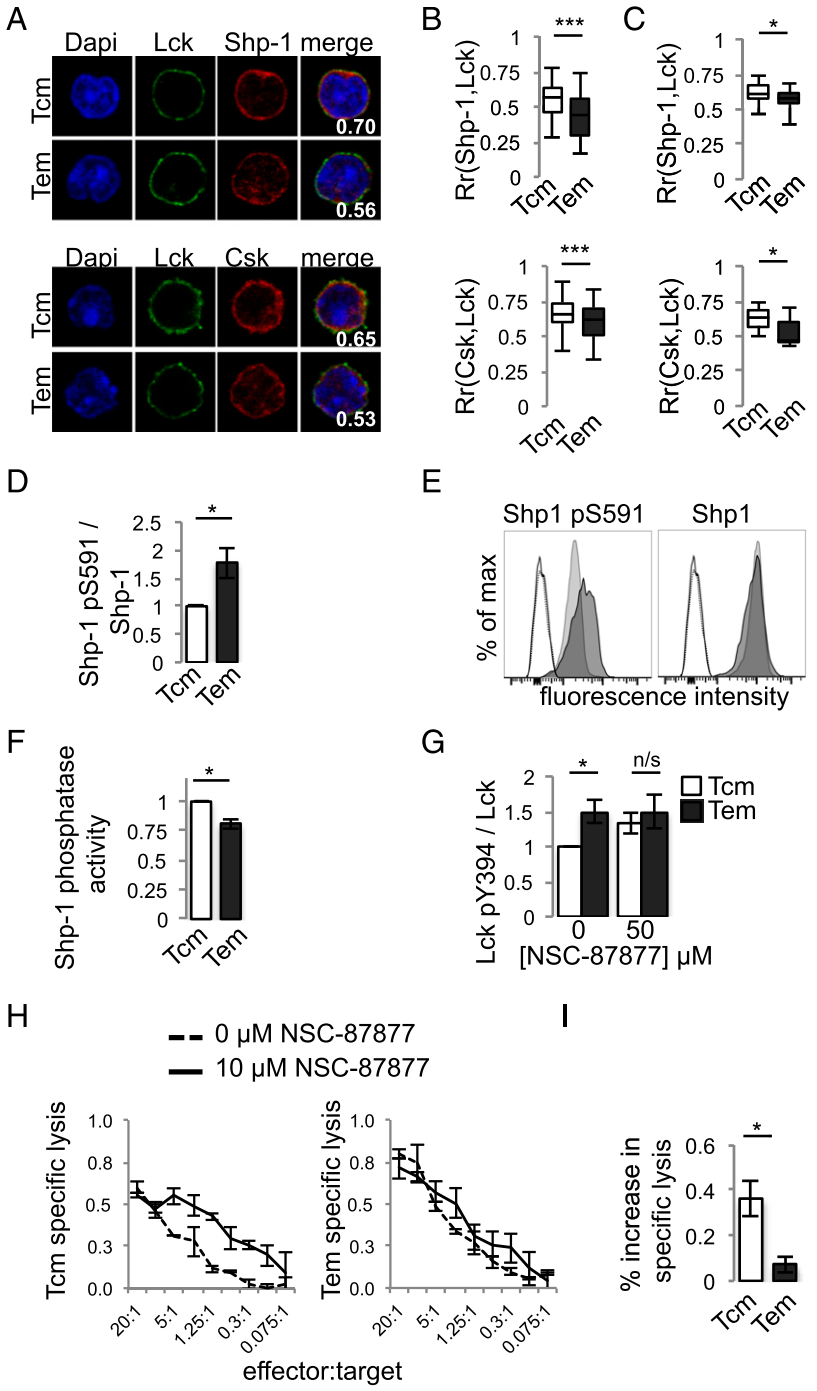

FIGURE 4. Shp-1 mediated differences in Lck activity between T_{CM} and T_{EM}. (**A**) JR209 T_{CM} and T_{EM} stained for Lck (green), DAPI (blue), and either Shp-1 (*top*) or Csk (*bottom*) (red). Original magnification ×63. (**B**) Pearson correlation coefficient (R_r) for Lck–Shp-1 (*top*) and Lck-Csk (*bottom*). Representative images in (A) display individually calculated R_r (for Lck–Shp-1: mean values, T_{CM} = 0.55, T_{EM} = 0.44; T_{CM} n = 53, T_{EM} n = 51. Mann–Whitney U test, p = 0.0003. For Lck-Csk: mean values, T_{CM} = 0.66, T_{EM} = 0.60; T_{CM} n = 115, T_{EM} n = 123. Mann–Whitney U test, p = 0.0004). (**C**) R_r for Lck–Shp-1 (*top*) and Lck-Csk (*bottom*) in in vivo–generated JR209 T_{CM} and T_{EM} (for Lck-Shp-1: mean values, T_{CM} = 0.62, T_{EM} = 0.57; T_{CM} n = 47, T_{EM} n = 17. Mann–Whitney U test, p = 0.045; for Lck-Csk: mean values, T_{CM} = 0.62, T_{EM} = 0.53; T_{CM} n = 25, T_{EM} n = 8. Mann–Whitney U test, p = 0.023). (**D**) Western blot analysis of phosphorylated Shp-1 S591 (n = 4, two-tailed t test, p = 0.045). (**E**) Flow cytometry quantification of phosphorylated Shp-1 S591 (*left*) and Shp-1 (*right*) in in vivo–generated JR209 T_{CM} (light, filled) and T_{EM} (dark, filled). Unfilled profiles represent secondary Ab only controls for T_{CM} (dashed line) and T_{EM} (solid line). (**F**) Analysis of Shp-1 phosphatase activity was determined by immunoprecipitation of Shp-1 and incubation with *p*-nitrophenyl phosphate, addition of 1 N NaOH, and OD measurement at 410 nm. Phosphatase activity was calculated as OD 410 nm divided by the amount of immunoprecipitated Shp-1, as quantified by Western blot, normalized to unity for T_{CM} (n = 3, two-tailed t test, p = 0.013). (**G**) Western blot analysis of pLck Y394 following overnight culture with indicated concentrations of Shp-1 inhibitor NSC-87877 (for 0 μM NSC-87877, both T_{CM} and T_{EM} n = 13; for 50 μM NSC-87877, both T_{CM} and T_{EM} n = 6; for 0 μM NSC-87877, two-tailed t test, p = 0.007, for 50 μM NSC-87877, two-tailed t test, p = 0.63). (**H**) Cytotoxic properties of JR209 T_{CM} (*left*) and T_{EM} (*right*) toward T2-A2Kb APCs loaded with 10 μM $gp100_{209–217(2M)}$ at E:T ratios indicated, following overnight culture with (solid line) or without (dashed line) 50 μM Shp-1 inhibitor NSC-87877. Plot is representative of triplicate experiments. Specific lysis was calculated as described in *Materials and Methods*. (**I**) The percentage changes in specific lysis of T_{CM} and T_{EM} following treatment with Shp-1 inhibitor NSC-87877 toward T2-A2Kb APCs loaded with 10 μM $gp100_{209–217(2M)}$ at 2.5:1 E:T ratio following overnight culture with 50 μM Shp-1 inhibitor NSC-87877. Specific lysis was calculated as described in *Materials and Methods* (n = 3, two-tailed t test, p = 0.029). *$p < 0.05$, ***$p < 0.001$.

A great deal is understood about the complex T cell activation signaling network, yet a universal model of T cell activation that accounts for its sensitivity and selectivity remains elusive (62). The Lck come&stay/signal duration model (14) improves upon the kinetic proofreading model (44), which posits that following ligation the TCR complex must undergo a series of steps prior to initiation of downstream activation signaling, enabling discrimination between Ags with small affinity differences. Significantly, the model predicts that coreceptor-mediated Lck recruitment to the pMHC–TCR complex is the most proximal limiting step in this process, and it predicts that the degree of coupling between active Lck and coreceptor strongly influences the probability of active Lck recruitment to the pMHC–TCR complex (14). Accordingly, evaluating the differences in Lck activity between T_{CM} and T_{EM} with this model predicts T_{EM} to have an increased probability of forming an active TCR complex following ligation compared with T_{CM} (Fig. 3G). T cell activation models such as the Lck come&stay/signal duration model (14) presume that Lck activity is not significantly altered following TCR ligation, which suggests that constitutive Lck activity would be an important factor in the initiation of downstream activation signaling (14), and differences in levels of Lck activity between T_{CM} and T_{EM} would be sufficient to alter the probabilities of achieving threshold signaling for T cell activation. This is supported by recent work by Manz et al. (13), which used titration of a Csk-specific inhibitor to induce a 3- to 4-fold increase in Lck Y394 phosphorylation in $CD8^+$ T cells. Importantly, whereas increased Lck activity led to weak phosphorylation of signaling molecules downstream of

Downloaded from http://www.jimmunol.org/ by guest on October 21, 2020

Zap-70, coupling this with TCR stimulation led to enhanced downstream signaling whose magnitude correlated with Lck Y394 phosphorylation (13). Their work therefore suggests that small changes in the amount of active Lck (as little as a 50% increase) can significantly affect the magnitude of activation signaling following TCR ligation. In our study, T_{EM} have significantly higher Lck Y394 phosphorylation than do T_{CM} (54% of Lck molecules compared with 18% for T_{CM}, Fig. 3C, 3D) and, correspondingly, T_{EM} have a roughly 60% higher kinase activity (Fig. 3E, 3F), and would thus strongly influence the magnitude of activation signaling and the probability of achieving threshold levels of signaling to induce effector function.

Our results also show that T_{CM} and T_{EM} differ in Lck Y505 phosphorylation (Supplemental Fig. 3A, 3B), which may contribute to the overall differences in Lck activity between T_{CM} and T_{EM} (Fig. 3C, 3D). However, the inhibitory effect of Lck Y505 phosphorylation on Lck activity is overcome by simultaneous Lck Y394 phosphorylation (12). It is possible that higher levels of Lck Y505 phosphorylation in T_{CM} may actually decrease the rate of *trans*-autophosphorylation of Y394 (63) and therefore contribute to the lower levels of Lck pY394 observed in T_{CM}. Our observation that Csk and Lck are more colocalized in T_{CM} compared with T_{EM} may explain why T_{CM} have higher levels of Lck pY505. It has previously been shown that Csk is differentially distributed in naive versus Ag-experienced $CD8^+$ T cells, affecting Csk colocalization with Lck (64). The mechanism behind the differential localization of Csk is unclear, although evidence suggests that it is due to PTP activity and not dependent on Cbp phosphorylation (64), as our data also suggest (Supplemental Fig. 3B). It is conceivable that the membrane organization of Lck itself may determine the extent of its colocalization with Csk. The open, active conformation of Lck induces self-clustering (65), which may result in greater sequestration from Csk. Therefore, higher levels of Lck pY394 in T_{EM}, driven by differences in Shp-1 activity, could lead to greater clustering of Lck and resulting lower levels of Lck pY505 owing to decreased membrane interaction with Csk. However, it must be considered that other mechanisms may contribute to the differential colocalization of Csk with Lck.

Shp-1 has been shown to interact constitutively with Themis in a GRB2-dependent manner, and this complex associates with phosphorylated LAT to mediate negative feedback to dampen activation signaling (51). Interestingly, Paster et al. (51) showed that knocking down Themis expression had no effect of constitutive Lck activity, although it did have a significant effect on TCR-proximal signaling, presumably due to decreased recruitment of Shp-1 to LAT. Our results showing the importance of Shp-1 in establishing the differences in constitutive Lck activity between T_{CM} and T_{EM} suggest therefore that this is mediated by Shp-1 in a Themis-independent manner. Our data suggest that differences in Shp-1 S591 phosphorylation between T_{CM} and T_{EM} result in differential Shp-1 membrane localization and phosphatase activity, which affects the degree to which Shp-1 can interact with Lck and to which Shp-1 can dephosphorylate Lck Y394, respectively (52). Although basal Shp-1 serine phosphorylation has been observed in resting T cells, the mechanism controlling Shp-1 S591 phosphorylation remains unclear (52). Although protein kinase C has been implicated in mediating Shp-1 S591 phosphorylation (66), other recent evidence does not support a role for protein kinase C in Shp-1 S591 phosphorylation, or at the very least suggests that other basophilic kinases have a role (52). Thus, further investigation is warranted into the mechanism by which constitutive Shp-1 phosphatase activity is controlled in resting memory T cells and how this directly affects constitutive Lck activity.

Although it has been shown that Lck activity is not required for maintenance, in vitro function, and secondary activation in vivo of virus-specific $CD8^+$ memory T cell (67), our results suggest that Lck activity may be important in determining the sensitivity of self-antigen–specific $CD8^+$ memory T cells. The contribution of constitutive Lck activity to $CD8^+$ memory T cell sensitivity may therefore be dependent on the Ag. For example, the virus-specific memory responses induced by gp33-specific TCR-expressing T cells (K_D = 3 μM) (68) are independent of Lck activity (67). However, responses to lower affinity self-antigens, such as gp100 (K_D = 9.3 μM) (69), as described herein, may be Lck-dependent. Alternatively, it is possible that Lck activity may not be required for JR209 T_{CM} and T_{EM} to elicit responses to gp100, but that the presence of Lck confers a further degree of sensitivity and enables more robust and/or selective responses to self-antigens. A more comprehensive understanding of the role of Lck in memory T cell responses will contribute to the overall understanding of how T cell sensitivity is established at the most proximal stages of TCR signaling.

Our findings also provide insight into further optimization of the in vitro preparation of T cells for use in clinical adoptive cell therapy applications (70) to produce effective in vivo antitumor properties, including effective homing, proliferation, persistence, and target cell lysis. In a number of experimental systems, T_{CM} show superior antitumor responses compared with T_{EM} (7, 15, 71), despite lesser cytotoxic effector properties (8). Therefore, it is possible that T_{CM} antitumor responses may be improved further by targeting TCR-proximal signaling components that drive cytotoxic effector function sensitivity, including Shp-1. Taken together, understanding the contributions of T cell maturation state, TCR affinity/avidity, and activation signaling components to T cell effector function sensitivity will help to guide the selection and manipulation of the optimal antitumor T cells for adoptive immunotherapy. Our finding that differences in constitutive Lck activity between T_{CM} and T_{EM} lead to T_{EM} being better poised to initiate TCR-proximal signaling represents a mechanism by which altered preligation activation states of TCR-proximal signaling components can affect T cell activation sensitivity. As such, Lck may represent a potential target for modification of T cell sensitivity for targeted T cell therapies for cancer and autoimmune diseases.

Acknowledgments

We thank the New York University Flow Cytometry Core and New York University School of Medicine Division of Comparative Medicine for technical assistance. We thank Arup Chakraborty for critical reading of this manuscript.

Disclosures

The authors have no financial conflicts of interest.

References

1. Davis, M. M., M. Krogsgaard, J. B. Huppa, C. Sumen, M. A. Purbhoo, D. J. Irvine, L. C. Wu, and L. Ehrlich. 2003. Dynamics of cell surface molecules during T cell recognition. *Annu. Rev. Biochem.* 72: 717–742.
2. Hogquist, K. A., and S. C. Jameson. 2014. The self-obsession of T cells: how TCR signaling thresholds affect fate "decisions" and effector function. *Nat. Immunol.* 15: 815–823.
3. Richer, M. J., J. C. Nolz, and J. T. Harty. 2013. Pathogen-specific inflammatory milieux tune the antigen sensitivity of $CD8^+$ T cells by enhancing T cell receptor signaling. *Immunity* 38: 140–152.
4. Willinger, T., T. Freeman, H. Hasegawa, A. J. McMichael, and M. F. Callan. 2005. Molecular signatures distinguish human central memory from effector memory CD8 T cell subsets. *J. Immunol.* 175: 5895–5903.
5. Sallusto, F., J. Geginat, and A. Lanzavecchia. 2004. Central memory and effector memory T cell subsets: function, generation, and maintenance. *Annu. Rev. Immunol.* 22: 745–763.

Downloaded from http://www.jimmunol.org/ by guest on October 21, 2020

6. Wherry, E. J., V. Teichgräber, T. C. Becker, D. Masopust, S. M. Kaech, R. Antia, U. H. von Andrian, and R. Ahmed. 2003. Lineage relationship and protective immunity of memory CD8 T cell subsets. *Nat. Immunol.* 4: 225–234.
7. Klebanoff, C. A., L. Gattinoni, P. Torabi-Parizi, K. Kerstann, A. R. Cardones, S. E. Finkelstein, D. C. Palmer, P. A. Antony, S. T. Hwang, S. A. Rosenberg, et al. 2005. Central memory self/tumor-reactive $CD8^+$ T cells confer superior antitumor immunity compared with effector memory T cells. *Proc. Natl. Acad. Sci. USA* 102: 9571–9576.
8. Gattinoni, L., C. A. Klebanoff, D. C. Palmer, C. Wrzesinski, K. Kerstann, Z. Yu, S. E. Finkelstein, M. R. Theoret, S. A. Rosenberg, and N. P. Restifo. 2005. Acquisition of full effector function in vitro paradoxically impairs the in vivo antitumor efficacy of adoptively transferred $CD8^+$ T cells. *J. Clin. Invest.* 115: 1616–1626.
9. Klebanoff, C. A., L. Gattinoni, and N. P. Restifo. 2006. $CD8^+$ T-cell memory in tumor immunology and immunotherapy. *Immunol. Rev.* 211: 214–224.
10. Straus, D. B., and A. Weiss. 1992. Genetic evidence for the involvement of the lck tyrosine kinase in signal transduction through the T cell antigen receptor. *Cell* 70: 585–593.
11. Iwashima, M., B. A. Irving, N. S. van Oers, A. C. Chan, and A. Weiss. 1994. Sequential interactions of the TCR with two distinct cytoplasmic tyrosine kinases. *Science* 263: 1136–1139.
12. Nika, K., C. Soldani, M. Salek, W. Paster, A. Gray, R. Etzensperger, L. Fugger, P. Polzella, V. Cerundolo, O. Dushek, et al. 2010. Constitutively active Lck kinase in T cells drives antigen receptor signal transduction. *Immunity* 32: 766–777.
13. Manz, B. N., Y. X. Tan, A. H. Courtney, F. Rutaganira, E. Palmer, K. M. Shokat, and A. Weiss. 2015. Small molecule inhibition of Csk alters affinity recognition by T cells. *eLife* 4: 4.
14. Stepanek, O., A. S. Prabhakar, C. Osswald, C. G. King, A. Bulek, D. Naeher, M. Beaufils-Hugot, M. L. Abanto, V. Galati, B. Hausmann, et al. 2014. Coreceptor scanning by the T cell receptor provides a mechanism for T cell tolerance. *Cell* 159: 333–345.
15. Klebanoff, C. A., S. E. Finkelstein, D. R. Surman, M. K. Lichtman, L. Gattinoni, M. R. Theoret, N. Grewal, P. J. Spiess, P. A. Antony, D. C. Palmer, et al. 2004. IL-15 enhances the in vivo antitumor activity of tumor-reactive $CD8^+$ T cells. *Proc. Natl. Acad. Sci. USA* 101: 1969–1974.
16. Yu, Z., M. R. Theoret, C. E. Touloukian, D. R. Surman, S. C. Garman, L. Feigenbaum, T. K. Baxter, B. M. Baker, and N. P. Restifo. 2004. Poor immunogenicity of a self/tumor antigen derives from peptide-MHC-I instability and is independent of tolerance. *J. Clin. Invest.* 114: 551–559.
17. Manjunath, N., P. Shankar, J. Wan, W. Weninger, M. A. Crowley, K. Hieshima, T. A. Springer, X. Fan, H. Shen, J. Lieberman, and U. H. von Andrian. 2001. Effector differentiation is not prerequisite for generation of memory cytotoxic T lymphocytes. *J. Clin. Invest.* 108: 871–878.
18. Schluns, K. S., and L. Lefrançois. 2003. Cytokine control of memory T-cell development and survival. *Nat. Rev. Immunol.* 3: 269–279.
19. Kim, S., S. Lee, J. Shin, Y. Kim, I. Evnouchidou, D. Kim, Y. K. Kim, Y. E. Kim, J. H. Ahn, S. R. Riddell, et al. 2011. Human cytomegalovirus microRNA miR-US4-1 inhibits $CD8^+$ T cell responses by targeting the aminopeptidase ERAP1. *Nat. Immunol.* 12: 984–991.
20. Romain, G., V. Senyukov, N. Rey-Villamizar, A. Merouane, W. Kelton, I. Liadi, A. Mahendra, W. Charab, G. Georgiou, B. Roysam, et al. 2014. Antibody Fc engineering improves frequency and promotes kinetic boosting of serial killing mediated by NK cells. *Blood* 124: 3241–3249.
21. Liadi, I., H. Singh, G. Romain, N. Rey-Villamizar, A. Merouane, J. R. Adolacion, P. Kebriaei, H. Huls, P. Qiu, B. Roysam, et al. 2015. Individual motile $CD4^+$ T cells can participate in efficient multikilling through conjugation to multiple tumor cells. *Cancer Immunol. Res.* 3: 473–482.
22. Merouane, A., N. Rey-Villamizar, Y. Lu, I. Liadi, G. Romain, J. Lu, H. Singh, L. J. Cooper, N. Varadarajan, and B. Roysam. 2015. Automated profiling of individual cell-cell interactions from high-throughput time-lapse imaging microscopy in nanowell grids (TIMING). *Bioinformatics* 31: 3189–3197.
23. Huppa, J. B., M. Gleimer, C. Sumen, and M. M. Davis. 2003. Continuous T cell receptor signaling required for synapse maintenance and full effector potential. *Nat. Immunol.* 4: 749–755.
24. Krogsgaard, M., Q. J. Li, C. Sumen, J. B. Huppa, M. Huse, and M. M. Davis. 2005. Agonist/endogenous peptide-MHC heterodimers drive T cell activation and sensitivity. *Nature* 434: 238–243.
25. Artyomov, M. N., M. Lis, S. Devadas, M. M. Davis, and A. K. Chakraborty. 2010. CD4 and CD8 binding to MHC molecules primarily acts to enhance Lck delivery. *Proc. Natl. Acad. Sci. USA* 107: 16916–16921.
26. Altan-Bonnet, G., and R. N. Germain. 2005. Modeling T cell antigen discrimination based on feedback control of digital ERK responses. *PLoS Biol.* 3: e356.
27. Parkhurst, M. R., M. L. Salgaller, S. Southwood, P. F. Robbins, A. Sette, S. A. Rosenberg, and Y. Kawakami. 1996. Improved induction of melanoma-reactive CTL with peptides from the melanoma antigen gp100 modified at HLA-A*0201-binding residues. *J. Immunol.* 157: 2539–2548.
28. Vitiello, A., D. Marchesini, J. Furze, L. A. Sherman, and R. W. Chesnut. 1991. Analysis of the HLA-restricted influenza-specific cytotoxic T lymphocyte response in transgenic mice carrying a chimeric human-mouse class I major histocompatibility complex. *J. Exp. Med.* 173: 1007–1015.
29. Weninger, W., M. A. Crowley, N. Manjunath, and U. H. von Andrian. 2001. Migratory properties of naive, effector, and memory $CD8^+$ T cells. *J. Exp. Med.* 194: 953–966.
30. Kerkar, S. P., L. Sanchez-Perez, S. Yang, Z. A. Borman, P. Muranski, Y. Ji, D. Chinnasamy, A. D. Kaiser, C. S. Hinrichs, C. A. Klebanoff, et al. 2011. Genetic engineering of murine $CD8^+$ and $CD4^+$ T cells for preclinical adoptive immunotherapy studies. *J. Immunother.* 34: 343–352.
31. Yee, C., J. A. Thompson, D. Byrd, S. R. Riddell, P. Roche, E. Celis, and P. D. Greenberg. 2002. Adoptive T cell therapy using antigen-specific $CD8^+$ T cell clones for the treatment of patients with metastatic melanoma: in vivo persistence, migration, and antitumor effect of transferred T cells. *Proc. Natl. Acad. Sci. USA* 99: 16168–16173.
32. Dudley, M. E., J. R. Wunderlich, J. C. Yang, P. Hwu, D. J. Schwartzentruber, S. L. Topalian, R. M. Sherry, F. M. Marincola, S. F. Leitman, C. A. Seipp, et al. 2002. A phase I study of nonmyeloablative chemotherapy and adoptive transfer of autologous tumor antigen-specific T lymphocytes in patients with metastatic melanoma. *J. Immunother.* 25: 243–251.
33. von Holzen, U., M. Adamina, M. Bolli, W. P. Weber, P. Zajac, C. Groeper, A. Reschner, C. Feder, R. Schumacher, W. Marti, et al. 2005. Selective responsiveness to common γ chain cytokines in peripheral blood-derived cytotoxic T lymphocytes induced by Melan-A/MART-$1_{27–35}$targeted active specific immunotherapy. *Int. J. Cancer* 115: 248–255.
34. Kelso, A., E. O. Costelloe, B. J. Johnson, P. Groves, K. Buttigieg, and D. R. Fitzpatrick. 2002. The genes for perforin, granzymes A-C and IFN-γ are differentially expressed in single $CD8^+$ T cells during primary activation. *Int. Immunol.* 14: 605–613.
35. Jenkins, M. R., A. Tsun, J. C. Stinchcombe, and G. M. Griffiths. 2009. The strength of T cell receptor signal controls the polarization of cytotoxic machinery to the immunological synapse. *Immunity* 31: 621–631.
36. Isaaz, S., K. Baetz, K. Olsen, E. Podack, and G. M. Griffiths. 1995. Serial killing by cytotoxic T lymphocytes: T cell receptor triggers degranulation, re-filling of the lytic granules and secretion of lytic proteins via a non-granule pathway. *Eur. J. Immunol.* 25: 1071–1079.
37. Jameson, S. C., F. R. Carbone, and M. J. Bevan. 1993. Clone-specific T cell receptor antagonists of major histocompatibility complex class I-restricted cytotoxic T cells. *J. Exp. Med.* 177: 1541–1550.
38. Koniaras, C., F. R. Carbone, W. R. Heath, and A. M. Lew. 1999. Inhibition of naive class I-restricted T cells by altered peptide ligands. *Immunol. Cell Biol.* 77: 318–323.
39. Guy, C. S., K. M. Vignali, J. Temirov, M. L. Bettini, A. E. Overacre, M. Smeltzer, H. Zhang, J. B. Huppa, Y. H. Tsai, C. Lobry, et al. 2013. Distinct TCR signaling pathways drive proliferation and cytokine production in T cells. *Nat. Immunol.* 14: 262–270.
40. Irvine, D. J., M. A. Purbhoo, M. Krogsgaard, and M. M. Davis. 2002. Direct observation of ligand recognition by T cells. *Nature* 419: 845–849.
41. Purbhoo, M. A., D. J. Irvine, J. B. Huppa, and M. M. Davis. 2004. T cell killing does not require the formation of a stable mature immunological synapse. *Nat. Immunol.* 5: 524–530.
42. Baniyash, M., P. Garcia-Morales, E. Luong, L. E. Samelson, and R. D. Klausner. 1988. The T cell antigen receptor ζ chain is tyrosine phosphorylated upon activation. *J. Biol. Chem.* 263: 18225–18230.
43. Haluszczak, C., A. D. Akue, S. E. Hamilton, L. D. Johnson, L. Pujanauski, L. Teodorovic, S. C. Jameson, and R. M. Kedl. 2009. The antigen-specific $CD8^+$ T cell repertoire in unimmunized mice includes memory phenotype cells bearing markers of homeostatic expansion. *J. Exp. Med.* 206: 435–448.
44. McKeithan, T. W. 1995. Kinetic proofreading in T-cell receptor signal transduction. *Proc. Natl. Acad. Sci. USA* 92: 5042–5046.
45. Deenick, E. K., A. V. Gett, and P. D. Hodgkin. 2003. Stochastic model of T cell proliferation: a calculus revealing IL-2 regulation of precursor frequencies, cell cycle time, and survival. *J. Immunol.* 170: 4963–4972.
46. Li, Q. J., A. R. Dinner, S. Qi, D. J. Irvine, J. B. Huppa, M. M. Davis, and A. K. Chakraborty. 2004. CD4 enhances T cell sensitivity to antigen by coordinating Lck accumulation at the immunological synapse. *Nat. Immunol.* 5: 791–799.
47. Feinerman, O., J. Veiga, J. R. Dorfman, R. N. Germain, and G. Altan-Bonnet. 2008. Variability and robustness in T cell activation from regulated heterogeneity in protein levels. *Science* 321: 1081–1084.
48. Chiang, G. G., and B. M. Sefton. 2001. Specific dephosphorylation of the Lck tyrosine protein kinase at Tyr-394 by the SHP-1 protein-tyrosine phosphatase. *J. Biol. Chem.* 276: 23173–23178.
49. Chow, L. M., M. Fournel, D. Davidson, and A. Veillette. 1993. Negative regulation of T-cell receptor signalling by tyrosine protein kinase $p50^{csk}$. *Nature* 365: 156–160.
50. Kawabuchi, M., Y. Satomi, T. Takao, Y. Shimonishi, S. Nada, K. Nagai, A. Tarakhovsky, and M. Okada. 2000. Transmembrane phosphoprotein Cbp regulates the activities of Src-family tyrosine kinases. *Nature* 404: 999–1003.
51. Paster, W., A. M. Bruger, K. Katsch, C. Grégoire, R. Roncagalli, G. Fu, N. R. Gascoigne, K. Nika, A. Cohnen, S. M. Feller, et al. 2015. A THEMIS: SHP1 complex promotes T-cell survival. *EMBO J.* 34: 393–409.
52. Liu, Y., M. J. Kruhlak, J. J. Hao, and S. Shaw. 2007. Rapid T cell receptor-mediated SHP-1 S591 phosphorylation regulates SHP-1 cellular localization and phosphatase activity. *J. Leukoc. Biol.* 82: 742–751.
53. Lorenz, U. 2009. SHP-1 and SHP-2 in T cells: two phosphatases functioning at many levels. *Immunol. Rev.* 228: 342–359.
54. Zhang, Z., K. Shen, W. Lu, and P. A. Cole. 2003. The role of C-terminal tyrosine phosphorylation in the regulation of SHP-1 explored via expressed protein ligation. *J. Biol. Chem.* 278: 4668–4674.
55. Stromnes, I. M., C. Fowler, C. C. Casamina, C. M. Georgopolos, M. S. McAfee, T. M. Schmitt, X. Tan, T. D. Kim, I. Choi, J. N. Blattman, and P. D. Greenberg. 2012. Abrogation of SRC homology region 2 domain-containing phosphatase 1 in tumor-specific T cells improves efficacy of adoptive immunotherapy by enhancing the effector function and accumulation of short-lived effector T cells in vivo. *J. Immunol.* 189: 1812–1825.

Downloaded from http://www.jimmunol.org/ by guest on October 21, 2020

56. Wolint, P., M. R. Betts, R. A. Koup, and A. Oxenius. 2004. Immediate cytotoxicity but not degranulation distinguishes effector and memory subsets of $CD8^+$ T cells. *J. Exp. Med.* 199: 925–936.
57. Bachmann, M. F., P. Wolint, K. Schwarz, P. Jäger, and A. Oxenius. 2005. Functional properties and lineage relationship of $CD8^+$ T cell subsets identified by expression of IL-7 receptor α and CD62L. *J. Immunol.* 175: 4686–4696.
58. Bachmann, M. F., P. Wolint, K. Schwarz, and A. Oxenius. 2005. Recall proliferation potential of memory $CD8^+$ T cells and antiviral protection. *J. Immunol.* 175: 4677–4685.
59. Seder, R. A., P. A. Darrah, and M. Roederer. 2008. T-cell quality in memory and protection: implications for vaccine design. *Nat. Rev. Immunol.* 8: 247–258.
60. Au-Yeung, B. B., J. Zikherman, J. L. Mueller, J. F. Ashouri, M. Matloubian, D. A. Cheng, Y. Chen, K. M. Shokat, and A. Weiss. 2014. A sharp T-cell antigen receptor signaling threshold for T-cell proliferation. *Proc. Natl. Acad. Sci. USA* 111: E3679–E3688.
61. Lever, M., P. K. Maini, P. A. van der Merwe, and O. Dushek. 2014. Phenotypic models of T cell activation. *Nat. Rev. Immunol.* 14: 619–629.
62. Chakraborty, A. K., and A. Weiss. 2014. Insights into the initiation of TCR signaling. *Nat. Immunol.* 15: 798–807.
63. Hui, E., and R. D. Vale. 2014. In vitro membrane reconstitution of the T-cell receptor proximal signaling network. *Nat. Struct. Mol. Biol.* 21: 133–142.
64. Borger, J. G., A. Filby, and R. Zamoyska. 2013. Differential polarization of C-terminal Src kinase between naive and antigen-experienced $CD8^+$ T cells. *J. Immunol.* 190: 3089–3099.
65. Rossy, J., D. M. Owen, D. J. Williamson, Z. Yang, and K. Gaus. 2013. Conformational states of the kinase Lck regulate clustering in early T cell signaling. *Nat. Immunol.* 14: 82–89.
66. Jones, M. L., J. D. Craik, J. M. Gibbins, and A. W. Poole. 2004. Regulation of SHP-1 tyrosine phosphatase in human platelets by serine phosphorylation at its C terminus. *J. Biol. Chem.* 279: 40475–40483.
67. Tewari, K., J. Walent, J. Svaren, R. Zamoyska, and M. Suresh. 2006. Differential requirement for Lck during primary and memory $CD8^+$ T cell responses. *Proc. Natl. Acad. Sci. USA* 103: 16388–16393.
68. Boulter, J. M., N. Schmitz, A. K. Sewell, A. J. Godkin, M. F. Bachmann, and A. M. Gallimore. 2007. Potent T cell agonism mediated by a very rapid TCR/pMHC interaction. *Eur. J. Immunol.* 37: 798–806.
69. Zhong, S., K. Malecek, L. A. Johnson, Z. Yu, E. Vega-Saenz de Miera, F. Darvishian, K. McGary, K. Huang, J. Boyer, E. Corse, et al. 2013. T-cell receptor affinity and avidity defines antitumor response and autoimmunity in T-cell immunotherapy. *Proc. Natl. Acad. Sci. USA* 110: 6973–6978.
70. Restifo, N. P., M. E. Dudley, and S. A. Rosenberg. 2012. Adoptive immunotherapy for cancer: harnessing the T cell response. *Nat. Rev. Immunol.* 12: 269–281.
71. Berger, C., M. C. Jensen, P. M. Lansdorp, M. Gough, C. Elliott, and S. R. Riddell. 2008. Adoptive transfer of effector $CD8^+$ T cells derived from central memory cells establishes persistent T cell memory in primates. *J. Clin. Invest.* 118: 294–305.

Downloaded from http://www.jimmunol.org/ by guest on October 21, 2020